Differentiation of Hepatocellular Carcinoma from Intrahepatic Cholangiocarcinoma through MRI Radiomics

Ning Liu , Yao-Kun Wu , Yun-Yun Tao , Jing Zheng , Xiao-Hua Huang , Lin Yang * , Xiao-Ming Zhang

Posted Date: 31 August 2023

doi: 10.20944/preprints202308.2164.v1

Keywords: radiomics; magnetic resonance imaging; hepatocellular carcinoma; intrahepatic cholangiocarcinoma; differentiation

Article

Differentiation of Hepatocellular Carcinoma from Intrahepatic Cholangiocarcinoma through MRI Radiomics

Ning Liu, Yao-Kun Wu, Yun-Yun Tao, Jing Zheng, Xiao-Hua Huang, Lin Yang * and Xiao-Ming Zhang

Medical Imaging Key Laboratory of Sichuan Province; Interventional Medicine Center, Department of Radiology, Medical Research Center, Affiliated Hospital of North Sichuan Medical College, Nanchong, Sichuan 637000, P. R. China.

* Correspondence: to linyangmd@163.com.

Simple Summary: The noninvasive differentiation of hepatocellular carcinoma (HCC) from intrahepatic cholangiocarcinoma (ICC) remains challenging. In recent years, the number of studies on the application of radiomics in liver cancer has grown dramatically. However, there have been very few studies on the differentiation of HCC from ICC based on multisequence magnetic resonance imaging (MRI) radiomics. This study aimed to investigate the efficacy of a radiomic model based on preoperative fat suppression T_2-weighted imaging (FS-T_2WI) and dynamic contrast-enhanced MRI features in the arterial phase (A) and portal venous phase (P) for the differentiation of HCC from ICC.

Abstract: The purpose of this study was to investigate the efficacy of magnetic resonance imaging (MRI) radiomics in differentiating hepatocellular carcinoma (HCC) from intrahepatic cholangiocarcinoma (ICC). The clinical and MRI data of 129 pathologically confirmed HCC cases and 48 ICC cases from April 2016 to December 2021 at the Affiliated Hospital of North Sichuan Medical College were retrospectively analyzed. Included cases were randomly divided at a ratio of 7:3 into a training group of 124 cases (90 HCC cases and 34 ICC cases) and a validation group of 53 cases (39 HCC cases and 14 ICC cases). Radiomic features were extracted from axial fat-suppression T_2-weighted imaging (FS-T_2WI) and axial arterial-phase (A) and portal-venous-phase (P) dynamic contrast-enhanced MRI sequences, and the corresponding datasets were generated. The least absolute shrinkage and selection operator (LASSO) method was used to select the best radiomic features. Logistic regression was used to establish a radiomic model for each sequence (FS-T_2WI, A, and P models) and a joint model (M model) integrating the radiomic features of all the sequences. The performance of each model was evaluated using the area under the receiver operating characteristic curve (AUC). The AUC of the FS-T_2WI, A, P, and M models for distinguishing HCC from ICC was 0.693, 0.863, 0.818, and 0.914 in the training group and 0.690, 0.784, 0.727, and 0.802 in the validation group, respectively. The results of this study suggest that MRI-based radiomics may help noninvasively differentiate HCC from ICC. The model integrating the radiomic features of multiple sequences showed further improvement in performance.

Keywords: radiomics; hepatocellular carcinoma; intrahepatic cholangiocarcinoma; differentiation

1. Introduction

Hepatocellular carcinoma (HCC) and intrahepatic cholangiocarcinoma (ICC) are the most common types of primary liver cancer, with the former accounting for approximately 75%-85% [1-3], and their morbidity rates are increasing [4-8]. The treatment strategies for and prognosis of patients with HCC and ICC are very different [2, 3, 9-16]. Therefore, accurate preoperative discrimination between HCC and ICC is essential.

At present, the noninvasive differentiation of HCC from ICC remains challenging. The sensitivity and specificity of serum tumor markers, including alpha-fetoprotein (AFP) and carbohydrate antigen 19-9 (CA19-9), are unsatisfactory [17-20]. The presentation of HCC and ICC on dynamic contrast-enhanced computed tomography (CT) or magnetic resonance imaging (MRI) is

 doi:10.20944/preprints202308.2164.v1

mostly typical [21-24]. However, both HCC and ICC may occur in patients with chronic hepatitis, and imaging enhancement patterns may tend to be similar in some patients with both HCC and ICC [3, 25-29]. In addition, the enhancement may be unremarkable or atypical in some HCC cases (especially cases of small, hypovascular, or sclerosing HCC lesions) [30-32]. Traditional medical imaging analysis relies heavily on the physician's subjective judgment and is thus prone to misdiagnosis [33]. Liver biopsy remains the gold standard for the final diagnosis, but this invasive procedure is refused by some patients [34]. Therefore, a preoperative, noninvasive method for distinguishing HCC from ICC is urgently needed.

The rapid development of artificial intelligence in recent years has led to it playing an important role in personalized precision medicine. Based on existing medical imaging modalities such as CT and MRI, an emerging technique known as radiomics [35] can be used to convert intrinsic pathophysiological information that is invisible to the human eye into high-dimensional quantitative image features, which can then be used to perform tumor classification via an analysis of the relationship between these features and clinical/genetic data [35-37]. Studies have shown that radiomics exhibits unique advantages in classifying the disease and predicting the prognosis of patients with liver cancer [35, 38-52]. However, there have been very few studies on the differentiation of HCC from ICC based on multisequence MRI radiomics to date. In this paper, the efficacy of a radiomic model based on preoperative fat suppression T_2-weighted imaging (FS-T_2WI) and dynamic contrast-enhanced MRI features in the arterial phase (A) and portal venous phase (P) for the differentiation of HCC from ICC was investigated.

2. Materials and Methods

2.1. Patients

The preoperative MRI and clinical data of HCC and ICC patients treated at the Affiliated Hospital of North Sichuan Medical College from April 2016 to December 2021 were retrospectively analyzed. The inclusion criteria were as follows: (1) a pathological diagnosis of HCC or ICC; (2) multisequence MRI of the upper abdomen performed within 4 weeks prior to surgery; and (3) no antitumor-related treatment prior to the MRI scan.The exclusion criteria were as follows: (1) combined hepatocellular-cholangiocarcinoma (cHCC-CC); (2) incomplete data or poor MR image quality; and (3) lesion diameter <2 cm or unclear lesion contours. The data of 206 patients with primary liver cancer (145 with HCC and 61 with ICC) were collected, and 177 (129 with HCC and 48 with ICC) met the criteria and were finally enrolled in this study. The patients were randomly divided at a 7:3 ratio into a training group (n=124, 90 with HCC and 34 with ICC) and a validation group (n=53, 39 with HCC and 14 with ICC) (Figure 1).

Preprints (www.preprints.org) | NOT PEER-REVIEWED | Posted: 31 August 2023 doi:10.20944/preprints202308.2164.v1

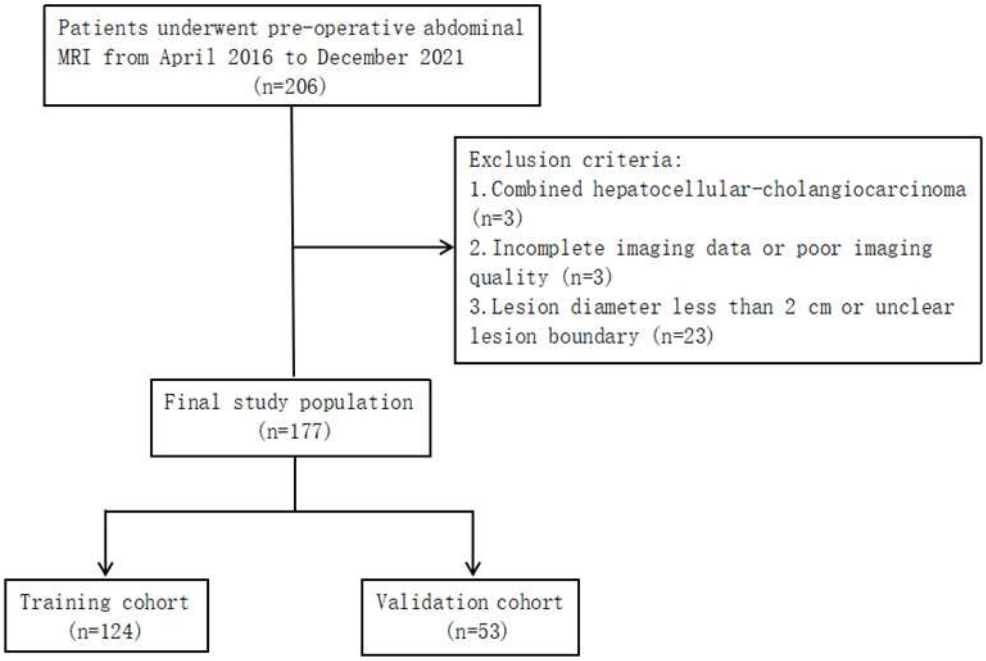

Figure 1. Flow chart of the study population.

The following clinical data were acquired: age; sex; cirrhosis status; hepatitis B serological test results; pseudocapsule status; hemorrhagic necrosis status; extrahepatic metastasis status; portal vein tumor thrombus status; number of tumors; ascites status; intrahepatic bile duct dilatation status; maximum tumor diameter; abnormal prothrombin; AFP level; carcinoembryonic antigen (CEA) level; and CA19-9 level. The levels of tumor markers were measured within one week before surgery.

2.2. MRI Acquisition

MRI scans were performed using a Discovery 750 3.0 T superconductivity MRI scanner with a 32-channel phased-array surface coil (GE, USA). Prior to the MRI scans, all subjects fasted for 4 hours and received training in breathing exercises. Scan sequences included axial 3D liver acceleration volume acquisition (LAVA), FS-T_2WI, and axial 3D LAVA dynamic contrast-enhanced sequences (Table 1). Gd-DTPA at a dose of 15-20 mL was used as the contrast agent for dynamic contrast enhancement and injected into the dorsal vein of the hand at 2-2.5 mL/s using a high-pressure syringe.

Table 1. MRI sequence and parameters.

Sequence	TR/TE (ms)	FA (°)	Matrix (mm^2)	FOV (mm^2)	ST (mm)
BH Ax LAVA-Flex	4/2	12	260×192	320×320–360×360	2.6
RTr Ax fs T_2WI	2,609/97	110	384×384	320×320–380×380	5
BH Ax LAVA-Flex+C	4/2	12	224×192	320×320–360×360	5

Notes: TR, repetition time; TE, echo time; FA, flip angle; FOV, field of view; ST, section thickness; LAVA-Flex, liver acquisition with volume acceleration flexible.

2.3. Image Segmentation and Feature Extraction

The MR images of patients were imported in DICOM format into IBEX software (β1.0, http://bit.ly/IBEX_MDAnderson) for tumor image segmentation. The entire tumor volume was manually delineated as a region of interest (ROI) along the edge of the lesion layer by layer on axial

 doi:10.20944/preprints202308.2164.v1

FS-T_2W as well as A and P images if the clinical and pathological data of the patients were unknown (Figure 2). The gray-level run-length matrix (GLRLM), gray-level cooccurrence matrix (GLCM), intensity histogram and shape features were extracted and used to construct the FS-T_2WI, A, and P datasets.

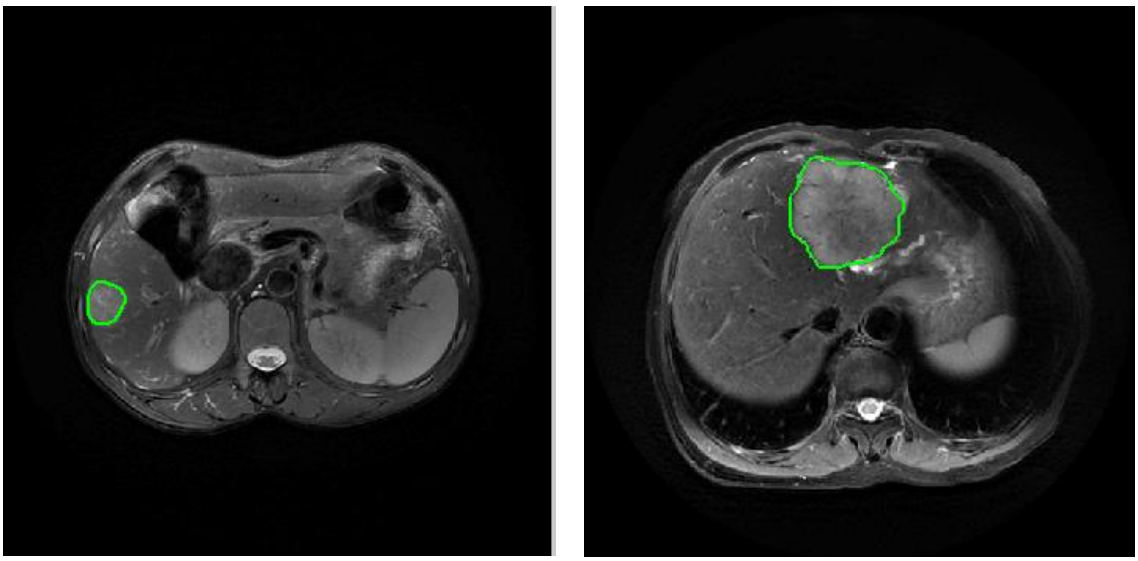

(A) (B)

Figure 2. Delineation of the ROI along the edge of the lesion: (A) HCC; (B) ICC.

2.4. Feature Selection

Sixty-one patients (42 with HCC and 19 with ICC) were randomly selected for intra- and intergroup consistency analysis. Interobserver consistency was assessed by comparing the segmentation results of two radiologists (observers 1 and 2, with 5 and 6 years of experience, respectively). Intraobserver consistency was assessed by comparing the segmentation results obtained by observer 2 more than one week after the initial results were obtained. The intraclass correlation coefficient was used to assess interobserver consistency, with a coefficient ≥0.75 considered to indicate good consistency. To eliminate discrepancies in the index dimension, all data were standardized by Z score. The dataset generated by each sequence was subjected to intra- and interobserver consistency tests. Features with an intraclass correlation coefficient <0.75 were eliminated.

From the stable features that remained, statistically significant features in differentiating HCC from ICC were selected using one-way statistical analysis (independent-samples *t* test or Mann–Whitney U test, according to the characteristics of the data distribution) (p<0.05). To avoid overfitting, least absolute shrinkage and selection operator (LASSO) regression analysis was performed to select the core radiomic features for differentiating HCC from ICC. The regularization parameter (λ) of the selected features was adjusted by 10-fold cross-validation using the 1-standard error (1-SE) method.

2.5. Model Establishment and Evaluation

The optimal radiomic features selected from each sequence were used to establish the radiomic models (FS-T_2WI, A, and P models) by logistic regression. By integrating the optimal features, a joint radiomic model (M) was established [41]. The efficacy of the models was assessed by the area under the receiver operating characteristic (ROC) curve (AUC), sensitivity, specificity, positive predictive value (PPV), negative predictive value (NPV), accuracy and F1 score as determined from the logistic regression confusion matrix.

Preprints (www.preprints.org) | NOT PEER-REVIEWED | Posted: 31 August 2023 doi:10.20944/preprints202308.2164.v1

2.6. Statistical Methods

R software (4.1.2, https://www.r-project.org/) was used for statistical data processing. Specifically, the software packages "psych", "glmnet", and "pROC" were used to assess the intergroup consistency of radiomic features, to perform LASSO regression analysis and to plot ROC curves, respectively. The normality and homogeneity of variance of the quantitative data were tested by the Shapiro–Wilk test and Bartlett test, respectively. The independent-samples *t* test was performed for quantitative data with a normal distribution and homogeneous variance; otherwise, the Mann–Whitney U test was performed. Quantitative data are described by the means or medians. Categorical variables were analyzed by the chi-square test and are described by percentages. Two-sided *p values* <0.05 was considered statistically significant.

3. Results

3.1. Patient Characteristics

Among the 177 patients, 129 had HCC (112 men and 17 women), and 48 had ICC (19 men and 29 women). Cirrhosis occurred in 121 patients (107 with HCC and 14 with ICC), and multinodular liver cancer occurred in 65 patients (47 with HCC and 18 with ICC). The maximum tumor diameter was 6.57±3.22 cm (Table 2).

Table 2. Patient clinical characteristics.

Parameter	Training cohort (*n*=124)	Validation cohort (*n*=53)	*P* value
Sex			
Male	94	38	0.565
Female	30	15	
Age			
≤60	78	32	0.751
>60	46	21	
Satellite nodules			
Yes	47	18	0.618
No	77	35	
Diameter			
≤5	41	25	0.076
>5	83	28	
Intrahepatic bile duct dilation			
Yes	31	14	0.843
No	93	39	
Ascites			
Yes	36	18	0.514
No	88	35	
Hemorrhagic necrosis			0.162
Yes	86	31	
No	38	22	
Pseudocapsule			0.975
Yes	26	11	

Preprints (www.preprints.org) | NOT PEER-REVIEWED | Posted: 31 August 2023 doi:10.20944/preprints202308.2164.v1

No	98	42	
Extrahepatic metastases			
Yes	23	6	0.234
No	101	47	
Portal vein tumor thrombus			0.445
Yes	35	18	
No	89	35	
Cirrhosis			
Yes	83	38	0.533
No	41	15	
Hepatitis B or C			
Yes	90	39	0.891
No	34	14	
AFP (ng/mL)			
<20	54	30	0.259
20~400	21	8	
>400	49	15	
DCP (mAU/mL)			
≤27.8	11	5	0.905
>27.8	113	48	
CA19-9 (U/mL)			
≤37	68	24	0.244
>37	56	29	
CEA (μg/L)			0.601
≤5	80	32	
>5	44	21	
Histologic result			
HCC	90	39	0.891
ICC	34	14	

Notes: HCC, hepatocellular carcinoma; ICC, intrahepatic cholangiocarcinoma; AFP, alpha-fetoprotein; CA19-9, carbohydrate antigen 19-9; DCP, des-gamma-carboxy prothrombin; CEA, carcinoembryonic antigen.

3.2. Feature Extraction and Selection

A total of 352 features were extracted from each of the FS-T_2WI, A and P datasets. Features with intra- and intergroup intraclass correlation coefficients <0.75 were eliminated, and the remaining features were further analyzed (Figure 3).

Preprints (www.preprints.org) | NOT PEER-REVIEWED | Posted: 31 August 2023 doi:10.20944/preprints202308.2164.v1

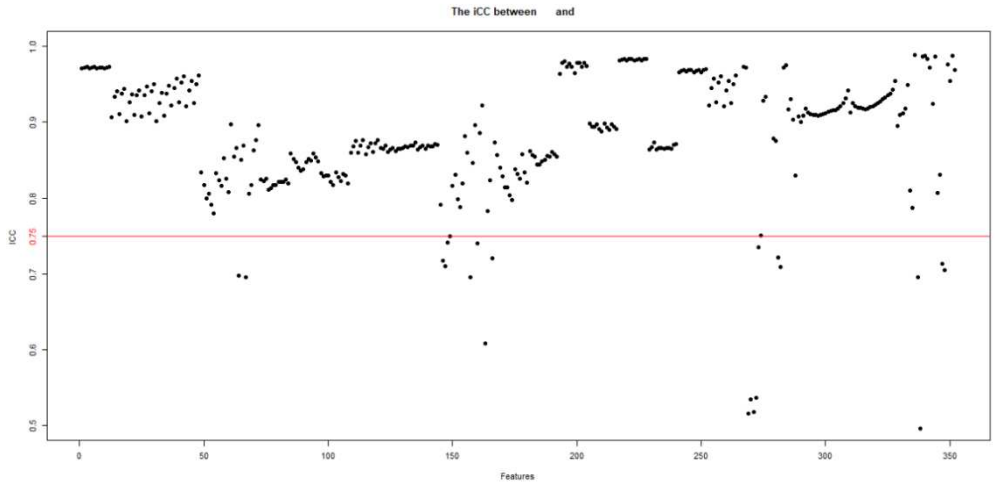

A1

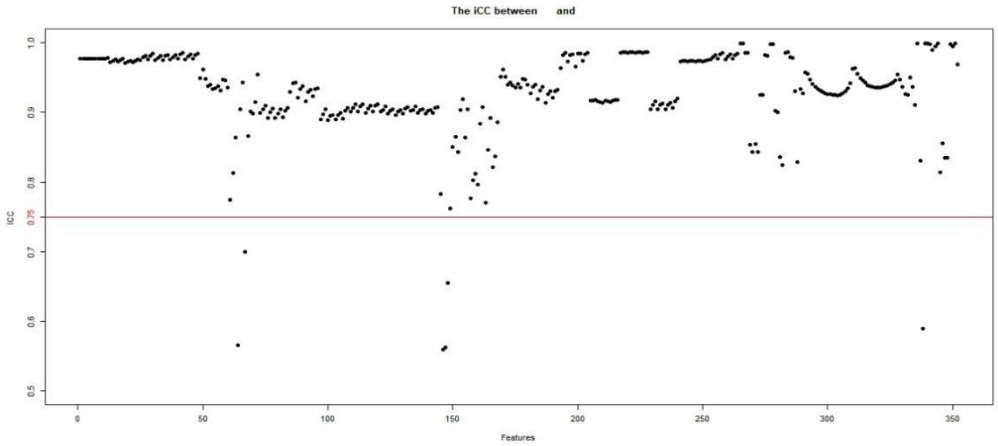

A2

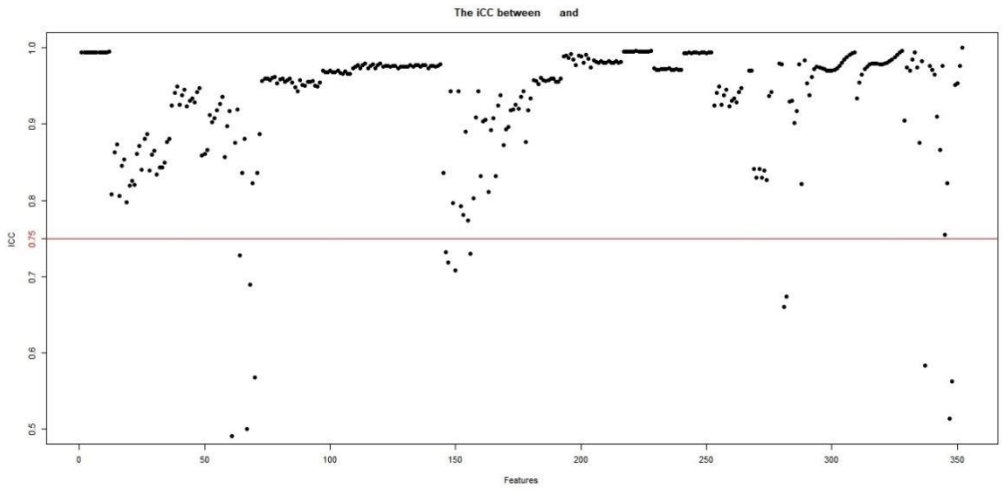

B1

Preprints (www.preprints.org) | NOT PEER-REVIEWED | Posted: 31 August 2023 doi:10.20944/preprints202308.2164.v1

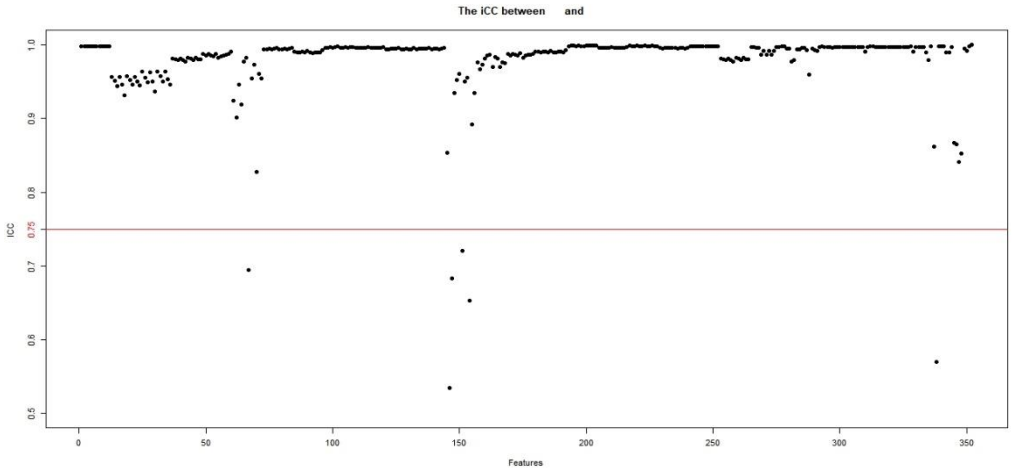

B2

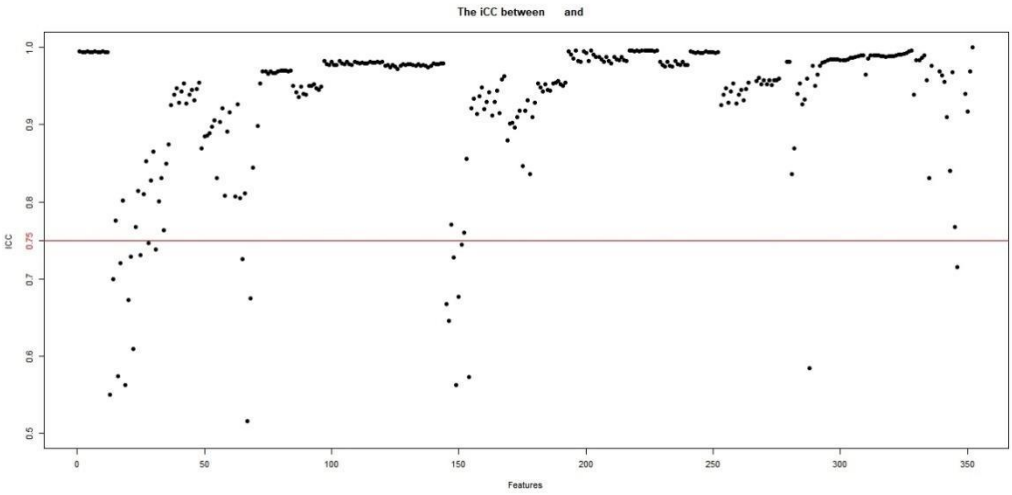

C1

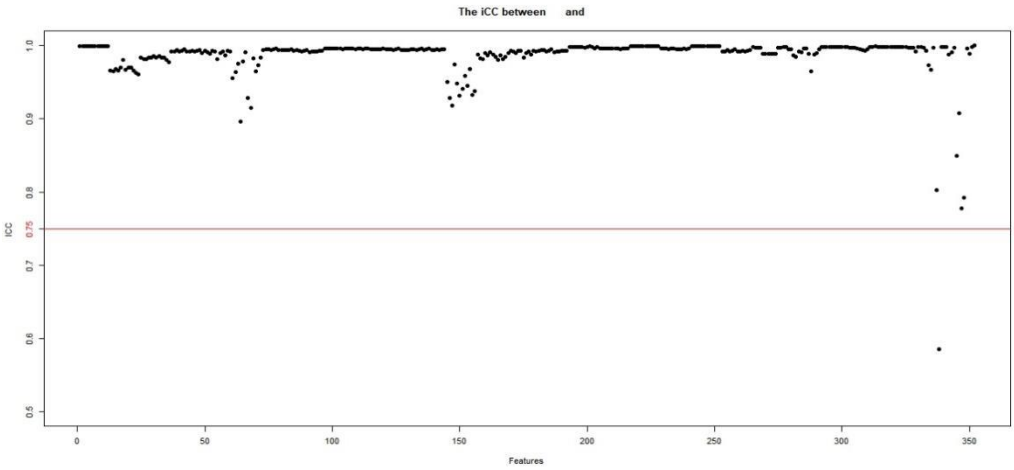

C2

Figure 3. Stability assessment of extracted MRI radiomic features by inter- and intraobserver intraclass correlation coefficients: (A1) intergroup FS-T_2WI; (A2) intragroup FS-T_2WI; (B1) intergroup arterial phase; (B2) intragroup arterial phase; (C1) intergroup portal venous phase; (C2) intragroup portal venous phase.

Preprints (www.preprints.org) | NOT PEER-REVIEWED | Posted: 31 August 2023 doi:10.20944/preprints202308.2164.v1

There were 327, 331 and 319 significantly different features in the FS-T2WI, A and P datasets, respectively (p<0.05), according to the independent-samples t test or Mann–Whitney U test. Finally, 1, 6 and 4 optimal features of these datasets were selected by LASSO regression, respectively (Figure 4 and Table 3).

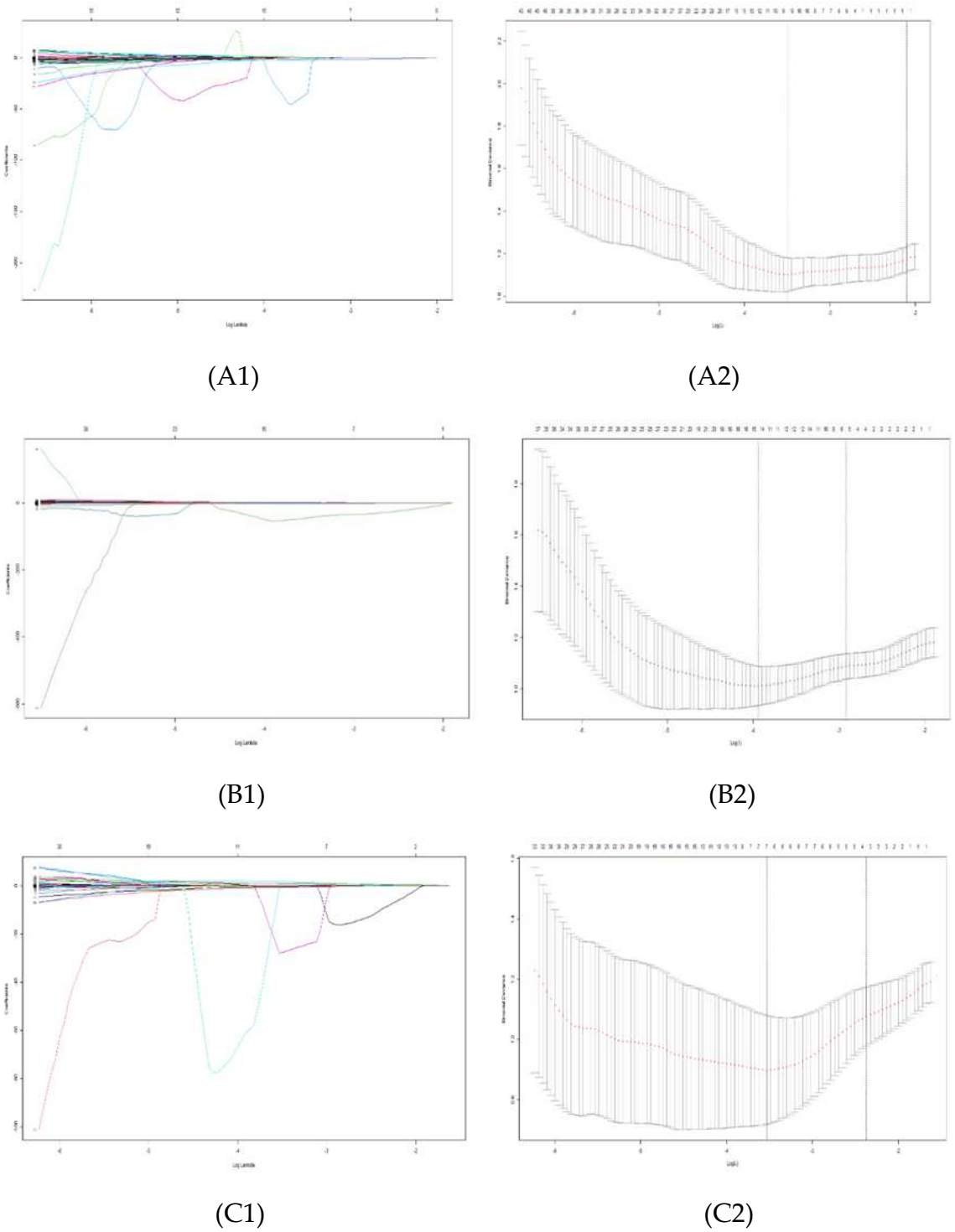

Figure 4. Feature selection using LASSO. (A1-A2) FS-T2WI; (B1-B2) arterial phase; (C1-C2) portal venous phase.

Preprints (www.preprints.org) | NOT PEER-REVIEWED | Posted: 31 August 2023 doi:10.20944/preprints202308.2164.v1

Table 3. Radiomic features for identifying HCC and ICC selected from each dataset by LASSO.

Cohort	Feature type	Feature name
FS-T2WI	Shape features (n=1)	Roundness
Arterial phase	Texture features (n=3)	
	GLCM (n=1)	45-7InverseDiffMomentNorm
	GLRLM (n=2)	0LongRunEmphasis
		90ShortRunLowGrayLevelEmpha
	Intensity histogram features (n=1)	InterQuartileRange
Portal vein phase	Shape features (n=2)	Mass
		Roundness
	Texture features (n=2)	
	GLCM (n=2)	90-1Contrast
		45-7InverseDiffMomentNorm
	Intensity histogram features (n=2)	InterQuartileRange
		MeanAbsoluteDeviation

Notes: HCC, hepatocellular carcinoma; ICC, intrahepatic cholangiocarcinoma; FS-T2WI, fat suppression T2-weighted imaging; GLCM, gray-level cooccurrence matrix; GLRLM, gray-level run-length matrix. GLCM features were constructed in four directions (θ = 0°, 45°, 90°, and 135°) and three offsets (d = 1, 4, 7); GLRLM features were constructed in two directions (θ = 0°, 90°) and one offset (d = 1).

3.3. Model Establishment and Evaluation

The above features selected from the FS-T2WI, A and P datasets were used to establish each radiomic model, and then the joint model (M model) was established by integrating the 11 features into a single model. The AUC of the FS-T2WI, A, P and M models was 0.693, 0.863, 0.818 and 0.914 in the training group and 0.690, 0.784, 0.727 and 0.802 in the validation group, respectively (Table 4 and Figure 5).

Table 4. Efficacy of each model in identifying HCC and ICC.

Cohort	Model	AUC	Sen	Spe	PPV	NPV	ACC	F1-score
Training	FS-T2WI model	0.693	0.147	0.956	0.556	0.748	0.734	0.233
	A model	0.863	0.588	0.933	0.769	0.857	0.839	0.667
	P model	0.818	0.588	0.922	0.741	0.856	0.831	0.656
	M model	0.914	0.706	0.922	0.774	0.892	0.863	0.738
Validation	FS-T2WI model	0.690	0.071	0.974	0.5	0.745	0.736	0.125
	A model	0.784	0.571	0.897	0.667	0.854	0.811	0.615
	P model	0.727	0.357	0.897	0.556	0.795	0.756	0.435
	M model	0.802	0.571	0.923	0.727	0.857	0.83	0.640

Notes: HCC, hepatocellular carcinoma; ICC, intrahepatic cholangiocarcinoma; FS-T2WI, fat suppression T2-weighted imaging; A, arterial phase; P, portal venous phase; M, multisequence joint; AUC, area under the receiver operating characteristic curve; ACC, accuracy; Sen, sensitivity; Spe, specificity; PPV, positive predictive value; NPV, negative predictive value.

Preprints (www.preprints.org) | NOT PEER-REVIEWED | Posted: 31 August 2023 doi:10.20944/preprints202308.2164.v1

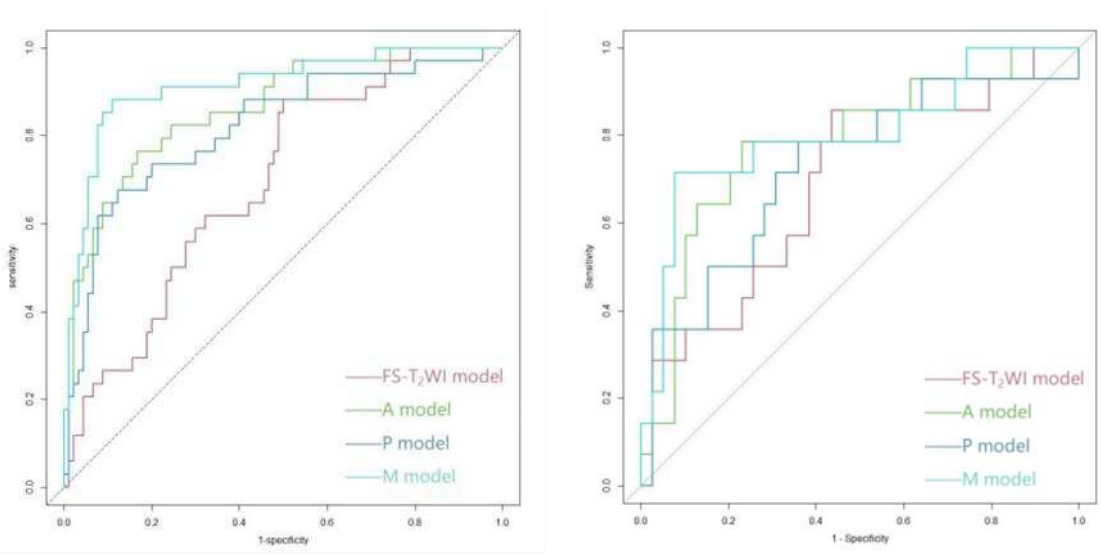

A B

Figure 5. Performance of the FS-T2WI model, A model, P model and M model in identifying HCC and ICC in the training group (A) and validation group (B) as detected by ROC curve analysis.

4. Discussion

MRI is characterized by high soft-tissue contrast, multiparametric and multidirectional imaging and a lack of radiation, making it the preferred imaging method for the identification and diagnosis of liver nodules [53, 54]. Dynamic contrast-enhanced MRI (DCE-MRI) is superior to dynamic contrast-enhanced CT in the detection and diagnosis of small HCC lesions (maximum diameter ≤2.0 cm) [55, 56]. Typical HCC displays significant heterogeneous enhancement in the arterial phase on DCE-MRI and reduced enhancement in the portal and/or parenchymal phase that is lower than that of normal liver parenchyma, resulting in a "fast-in and fast-out" enhancement pattern [21, 24]. In contrast, ICC shows less obvious enhancement or heterogeneous mild enhancement in the arterial phase on DCE-MRI that gradually increases with time [22, 23]. However, it is still difficult to differentiate HCC from ICC in clinical practice. Studies [26, 30-32] have shown that small ICC lesions (diameter<3 cm) and some ICC lesions in the setting of cirrhosis (approximately 7%) show the same enhancement pattern as typical HCC lesions, and approximately 10%-20% of HCC lesions (especially small, hypovascular, or sclerosing HCC lesions) show less obvious enhancement on imaging.

Choi et al. [57] conducted gadoxetic acid-enhanced MR and dynamic CT scans to identify HCC and ICC. The results showed that portal venous phase (PVP) washout instead of conventional washout in gadoxetic acid-enhanced MRI can prevent misidentification of HCC as ICC in patients with cirrhosis; however, it reduces the sensitivity of the method for identifying HCC. Diffusion-weighted imaging (DWI) reflects the diffusion of water molecules in tissues by measuring the apparent diffusion coefficient (ADC). Wei et al. [58] and Lewis et al. [59] found that the ADC can help differentiate HCC from ICC. However, ICC has multiple cellular origins and shares similar biological behaviors to some extent with HCC; thus, the ADC of ICC can partially overlap with that of HCC. Additionally, DWI does not display small lesions well because of the limited spatial resolution, and conventional DWI is based on a monoexponential model that cannot differentiate between water molecule diffusion and blood perfusion [60]. Intravoxel incoherent motion-DWI (IVIM-DWI) can simultaneously quantify the diffusion of water molecules and microcirculatory perfusion in living tissues. A previous study [61] showed that both the ADC and Dslow values were significantly lower in HCC than in ICC, but the Dfast value was significantly higher in HCC than in ICC; furthermore, Dfast was more efficient in the differential diagnosis of HCC and ICC, and there was no significant difference in the f value between Dfast and Dslow. The value of IVIM-DWI in identifying HCC and ICC has also been reported by other scholars [58, 62, 63]. However, the conclusion regarding D_{fast} and

f in distinguishing HCC from ICC remains inconsistent or controversial; thus, further research is needed. As an effective tumor imaging tool, positron emission tomography (PET)-MRI can play a role in patient management. Çelebi et al. [64] argued that PET-MRI using ^{18}F-fluorodeoxyglucos (^{18}F-FDG) as a tracer agent can help differentiate between HCC and ICC. However, there is a need to deeply explore whether there are great differences in FDG uptake between HCC and ICC, the accuracy of identification in some challenging cases (e.g., specific subgroups of patients in which the standard uptake value (SUV) is not a determining factor), and the optimal imaging sequence and model.

To date, few studies have investigated the differentiation of HCC from ICC based on MRI radiomics [38, 40, 59, 65]. Liu et al. [40] adopted machine learning-based CT and MR image features in the identification of cHCC-CC, ICC and HCC. The results showed that MRI features had the highest efficacy in differentiating between cHCC-CC and non-cHCC-CC, while CT features were less valuable. Moreover, precontrast- and portal-phase CT features were superior to enhanced MRI features in differentiating between HCC and non-HCC (AUC=0.79-0.81 for MRI, 0.81 for precontrast-phase CT and 0.71 for portal-phase CT). Wang et al. [65] used MRI radiomics to preoperatively identify cHCC-CC, HCC and ICC and found that the performance of the higher-order feature-based model was better than that of the lower-order feature-based model by approximately 10% and that the former performed better in identifying HCC in the delayed phase. Lewis et al. [59] extracted first-order radiomic features from ADC data and evaluated the ability of these features and the Liver Imaging Reporting and Data System (LI-RADS) classification to differentiate HCC, ICC and cHCC-CC. The results revealed that the AUC of the combination of sex, LI-RADS grade and the fifth percentile of the ADC in the diagnosis of HCC was 0.90 and 0.89 for two independent observers, respectively,. T_2*WI can reflect the magnetic susceptibility variation in tissues and thus be used to assess the biological properties of tumor tissues [66]. Huang et al. [38] extracted radiomic features from T_2*W images and then established radiomic nomogram models combined with clinical risk factors to distinguish between HCC and ICC. The results showed that the AUC of the radiomic model was 0.90 and 0.91 in the training and validation groups, respectively; the AUC of clinical features was 0.88 in the training group and 0.83 in the validation group, and the AUC of the radiomic nomogram was 0.97 and 0.95 in the training and validation groups, respectively. Similar results were obtained by Zhou et al. [39]. However, the efficacy of a joint model incorporating multiple sequence features was not investigated in these studies.

Different kinds of information related to tumor structure can be revealed by different sequences: T_2WI exhibits the underlying tumor morphology and heterogeneity, and enhancement scans can reflect differences in the tumor blood supply. In this work, enhancements in the arterial and venous phases were combined based on T_2WI to explore the efficacy of a joint model according to the blood supply status and enhancement patterns of HCC and ICC. The results showed that while each model had the potential to identify HCC and ICC in both the training and validation groups, the joint model incorporating multiple sequence features showed the highest efficacy [40, 65]. The AUC of the T2WI model was relatively low in this study, consistent with the findings of Liu et al. [67]. Therefore, the value of FS-T_2WI-based radiomics in distinguishing between HCC and ICC remains to be properly determined pending further research.

The radiomic features selected in this study were mainly GLCM and GLRLM features, textural features used to quantify tumor heterogeneity by reflecting the relationship between adjacent voxels/pixels [68], which is consistent with the results of related studies [38, 40, 69-74]. Histogram features show the global distribution of grayscale values in the image and can also be used to assess tumor heterogeneity [75]; Lewis et al. [59] found that the 5th/10th/95th percentiles of the ADC could significantly differentiate HCC from ICC and cHCC-CC. Shape features reflect the geometric characteristics of tumors [68]; Zhao et al. [76] confirmed that HCC tends to be more spherical than ICC in terms of morphology.

This study had the following limitations. (1) In this retrospective study, many HCC and ICC patients who did not undergo preoperative MRI scans were excluded, so there may be a potential selection bias. (2) The sample was small and from a single center, and cHCC-CC and ICC types other

than the mass-forming type were not included in the study. In the future, the sample size should be expanded to multiple centers for further model validation. (3) Other relevant MRI sequences were not analyzed, so their potential contributions might have been ignored.

5. Conclusions

Multisequence MRI radiomic models can be used to preoperatively distinguish between HCC and ICC, and the efficacy of these models can be further enhanced by including information from multiple sequences.

Author Contributions: N.L. and L.Y. wrote the paper. Y.-K.W., Y.-Y.T. and J.Z. collected the data. X.-H.H., L.Y. and X.-M.Z. designed the research. All authors have read and agreed to the published version of the manuscript.

Funding: This work was supported by the Project of City-University Science and Technology Strategic Cooperation of Nanchong City (No. 20SXQT0324).

Institutional Review Board Statement: The study was conducted in accordance with the Declaration of Helsinki and approved by the Ethics Committee of the Affiliated Hospital of North Sichuan Medical College (No. 2022ER545-1).

Informed Consent Statement: The requirement for patient consent was waived due to retrospective anonymous data collection without any risk to patients.

Data Availability Statement: The data presented in this study are available on request from the corresponding author.

Conflicts of Interest: The authors declare no conflicts of interest.

References

1. Sung H, Ferlay J, Siegel R L, et al. Global Cancer Statistics 2020: GLOBOCAN Estimates of Incidence and Mortality Worldwide for 36 Cancers in 185 Countries. [J]. CA: a cancer journal for clinicians, 2021,71(3):209-249.
2. Si Y, Wang X, Pan C, et al. An Efficient Nomogram for Discriminating Intrahepatic Cholangiocarcinoma From Hepatocellular Carcinoma: A Retrospective Study. [J]. Frontiers in oncology, 2022,12:833999.
3. Cheng N, Khoo N, Chung A Y F, et al. Pre-operative Imaging Characteristics in Histology-Proven Resected Intrahepatic Cholangiocarcinoma. [J]. World journal of surgery, 2020,44(11):3862-3867.
4. Florio A A, Ferlay J, Znaor A, et al. Global trends in intrahepatic and extrahepatic cholangiocarcinoma incidence from 1993 to 2012. [J]. Cancer, 2020,126(11):2666-2678.
5. Saha S K, Zhu A X, Fuchs C S, et al. Forty-Year Trends in Cholangiocarcinoma Incidence in the U.S.: Intrahepatic Disease on the Rise. [J]. The oncologist, 2016,21(5):594-599.
6. Valle J W, Borbath I, Khan S A, et al. Biliary cancer: ESMO Clinical Practice Guidelines for diagnosis, treatment and follow-up. [J]. Annals of oncology : official journal of the European Society for Medical Oncology, 2016,27(suppl 5):v28-v37.
7. Banales J M, Cardinale V, Carpino G, et al. Expert consensus document: Cholangiocarcinoma: current knowledge and future perspectives consensus statement from the European Network for the Study of Cholangiocarcinoma (ENS-CCA). [J]. Nat Rev Gastroenterol Hepatol, 2016,13(5):261-280.
8. Gupta A, Dixon E. Epidemiology and risk factors: intrahepatic cholangiocarcinoma. [J]. Hepatobiliary surgery and nutrition, 2017,6(2):101-104.
9. Nart D, Ertan Y, Pala E E, et al. Intrahepatic cholangiocarcinoma arising in chronic viral hepatitis-associated cirrhosis: two transplant cases. [J]. Transplant Proc, 2008,40(10):3813-3815.
10. Kelley R K, Bridgewater J, Gores G J, et al. Systemic therapies for intrahepatic cholangiocarcinoma. [J]. Journal of hepatology, 2020,72(2):353-363.
11. Banales J M, Iñarrairaegui M, Arbelaiz A, et al. Serum Metabolites as Diagnostic Biomarkers for Cholangiocarcinoma, Hepatocellular Carcinoma, and Primary Sclerosing Cholangitis. [J]. Hepatology (Baltimore, Md.), 2019,70(2):547-562.
12. Buettner S, van Vugt J L, IJzermans J N, et al. Intrahepatic cholangiocarcinoma: current perspectives. [J]. OncoTargets and therapy, 2017,10:1131-1142.
13. Liu W, Wang K, Bao Q, et al. Hepatic resection provided long-term survival for patients with intermediate and advanced-stage resectable hepatocellular carcinoma. [J]. World journal of surgical oncology, 2016,14:62.
14. Weber S M, Ribero D, O'Reilly E M, et al. Intrahepatic cholangiocarcinoma: expert consensus statement. [J]. HPB : the official journal of the International Hepato Pancreato Biliary Association, 2015,17(8):669-680.

15. Spolverato G, Kim Y, Alexandrescu S, et al. Is Hepatic Resection for Large or Multifocal Intrahepatic Cholangiocarcinoma Justified? Results from a Multi-Institutional Collaboration. [J]. Annals of surgical oncology, 2015,22(7):2218-2225.
16. Bruix J, Reig M, Sherman M. Evidence-Based Diagnosis, Staging, and Treatment of Patients With Hepatocellular Carcinoma [J]. Gastroenterology, 2016,150(4):835-853.
17. Huang D, Lin Q, Song J, et al. Prognostic Value of Pretreatment Serum CA199 in Patients with Locally Advanced Rectal Cancer Treated with CRT Followed by TME with Normal Pretreatment Carcinoembryonic Antigen Levels. [J]. Digestive surgery, 2021,38(1):24-29.
18. Qi F, Zhou A, Yan L, et al. The diagnostic value of PIVKA-II, AFP, AFP-L3, CEA, and their combinations in primary and metastatic hepatocellular carcinoma. [J]. J Clin Lab Anal, 2020,34(5):e23158.
19. Afshar M, Fletcher P, Bardoli A D, et al. Non-secretion of AFP and neutrophil lymphocyte ratio as predictors for survival in hepatocellular carcinoma patients treated with sorafenib: a large UK cohort. [J]. Oncotarget, 2018,9(24):16988-16995.
20. Teng D, Wu K, Sun Y, et al. Significant increased CA199 levels in acute pancreatitis patients predicts the presence of pancreatic cancer. [J]. Oncotarget, 2018,9(16):12745-12753.
21. Marrero J A, Kulik L M, Sirlin C B, et al. Diagnosis, Staging, and Management of Hepatocellular Carcinoma: 2018 Practice Guidance by the American Association for the Study of Liver Diseases. [J]. Hepatology (Baltimore, Md.), 2018,68(2):723-750.
22. Lafaro K J, Cosgrove D, Geschwind J H, et al. Multidisciplinary Care of Patients with Intrahepatic Cholangiocarcinoma: Updates in Management. [J]. Gastroenterology research and practice, 2015,2015:860861.
23. Hennedige T P, Neo W T, Venkatesh S K. Imaging of malignancies of the biliary tract- an update. [J]. Cancer imaging : the official publication of the International Cancer Imaging Society, 2014,14(1):14.
24. Liver E A F T, Cancer E O F R. EASL-EORTC clinical practice guidelines: management of hepatocellular carcinoma. [J]. Journal of hepatology, 2012,56(4):908-943.
25. Li R, Cai P, Ma K, et al. Dynamic enhancement patterns of intrahepatic cholangiocarcinoma in cirrhosis on contrast-enhanced computed tomography: risk of misdiagnosis as hepatocellular carcinoma. [J]. Sci Rep, 2016,6:26772.
26. Huang B, Wu L, Lu X, et al. Small Intrahepatic Cholangiocarcinoma and Hepatocellular Carcinoma in Cirrhotic Livers May Share Similar Enhancement Patterns at Multiphase Dynamic MR Imaging. [J]. Radiology, 2016,281(1):150-157.
27. Galassi M, Iavarone M, Rossi S, et al. Patterns of appearance and risk of misdiagnosis of intrahepatic cholangiocarcinoma in cirrhosis at contrast enhanced ultrasound. [J]. Liver Int, 2013,33(5):771-779.
28. Iavarone M, Piscaglia F, Vavassori S, et al. Contrast enhanced CT-scan to diagnose intrahepatic cholangiocarcinoma in patients with cirrhosis. [J]. Journal of hepatology, 2013,58(6):1188-1193.
29. Kim S J, Lee J M, Han J K, et al. Peripheral mass-forming cholangiocarcinoma in cirrhotic liver. [J]. AJR Am J Roentgenol, 2007,189(6):1428-1434.
30. Hanna R F, Aguirre D A, Kased N, et al. Cirrhosis-associated hepatocellular nodules: correlation of histopathologic and MR imaging features. [J]. Radiographics : a review publication of the Radiological Society of North America, Inc, 2008,28(3):747-769.
31. Choi S, Kim Y K, Min J H, et al. Added value of ancillary imaging features for differentiating scirrhous hepatocellular carcinoma from intrahepatic cholangiocarcinoma on gadoxetic acid-enhanced MR imaging. [J]. European radiology, 2018,28(6):2549-2560.
32. Chong Y S, Kim Y K, Lee M W, et al. Differentiating mass-forming intrahepatic cholangiocarcinoma from atypical hepatocellular carcinoma using gadoxetic acid-enhanced MRI. [J]. Clinical radiology, 2012,67(8):766-773.
33. Potretzke T A, Tan B R, Doyle M B, et al. Imaging Features of Biphenotypic Primary Liver Carcinoma (Hepatocholangiocarcinoma) and the Potential to Mimic Hepatocellular Carcinoma: LI-RADS Analysis of CT and MRI Features in 61 Cases [J]. American Journal of Roentgenology, 2016,207(1):25-31.
34. Losic B, Craig A J, Villacorta-Martin C, et al. Intratumoral heterogeneity and clonal evolution in liver cancer. [J]. Nature communications, 2020,11(1):291.
35. Lambin P, Rios-Velazquez E, Leijenaar R, et al. Radiomics: extracting more information from medical images using advanced feature analysis [J]. Eur J Cancer, 2012,48(4):441-446.
36. Tao Y, Shi Y, Gong X, et al. Radiomic Analysis Based on Magnetic Resonance Imaging for Predicting PD-L2 Expression in Hepatocellular Carcinoma. [J]. Cancers, 2023,15(2).
37. Mao Q, Zhou M, Zhao Z, et al. Role of radiomics in the diagnosis and treatment of gastrointestinal cancer. [J]. World journal of gastroenterology, 2022,28(42):6002-6016.
38. Huang F, Liu X, Liu P, et al. The Application Value of MRI T2* WI Radiomics Nomogram in Discriminating Hepatocellular Carcinoma from Intrahepatic Cholangiocarcinoma [J]. Computational and Mathematical Methods in Medicine, 2022,2022:1-13.

39. Zhou Y, Zhou G, Zhang J, et al. DCE-MRI based radiomics nomogram for preoperatively differentiating combined hepatocellular-cholangiocarcinoma from mass-forming intrahepatic cholangiocarcinoma. [J]. European radiology, 2022,32(7):5004-5015.
40. Liu X, Khalvati F, Namdar K, et al. Can machine learning radiomics provide pre-operative differentiation of combined hepatocellular cholangiocarcinoma from hepatocellular carcinoma and cholangiocarcinoma to inform optimal treatment planning? [J]. European Radiology, 2021,31(1):244-255.
41. Wang W, Gu D, Wei J, et al. A radiomics-based biomarker for cytokeratin 19 status of hepatocellular carcinoma with gadoxetic acid-enhanced MRI. [J]. European radiology, 2020,30(5):3004-3014.
42. Mokrane F, Lu L, Vavasseur A, et al. Radiomics machine-learning signature for diagnosis of hepatocellular carcinoma in cirrhotic patients with indeterminate liver nodules. [J]. European radiology, 2020,30(1):558-570.
43. Jeong W K, Jamshidi N, Felker E R, et al. Radiomics and radiogenomics of primary liver cancers [J]. Clinical and Molecular Hepatology, 2019,25(1):21-29.
44. Jiang H, Liu X, Chen J, et al. Man or machine? Prospective comparison of the version 2018 EASL, LI-RADS criteria and a radiomic odel to diagnose hepatocellular carcinoma. [J]. Cancer Imaging, 2019,19(1):84.
45. Hectors S J, Lewis S, Besa C, et al. MRI radiomics features predict immuno-oncological characteristics of hepatocellular carcinoma. [J]. European radiology, 2020,30(7):3759-3769.
46. Chen S, Feng S, Wei J, et al. Pretreatment prediction of immunoscore in hepatocellular cancer: a radiomics-based clinical model based on Gd-EOB-DTPA-enhanced MRI imaging [J]. European Radiology, 2019,29(8):4177-4187.
47. Yang L, Gu D, Wei J, et al. A Radiomics Nomogram for Preoperative Prediction of Microvascular Invasion in Hepatocellular Carcinoma. [J]. Liver cancer, 2019,8(5):373-386.
48. Nebbia G, Zhang Q, Arefan D, et al. Pre-operative Microvascular Invasion Prediction Using Multi-parametric Liver MRI Radiomics. [J]. Journal of digital imaging, 2020,33(6):1376-1386.
49. Ji G, Zhu F, Xu Q, et al. Machine-learning analysis of contrast-enhanced CT radiomics predicts recurrence of hepatocellular carcinoma after resection: A multi-institutional study. [J]. EBioMedicine, 2019,50:156-165.
50. Wang X, Long L, Cui Y, et al. MRI-based radiomic odel for preoperative prediction of 5-year survival in patients with hepatocellular carcinoma. [J]. British journal of cancer, 2020,122(7):978-985.
51. Lubner M G, Smith A D, Sandrasegaran K, et al. CT Texture Analysis: Definitions, Applications, Biologic Correlates, and Challenges. [J]. Radiographics : a review publication of the Radiological Society of North America, Inc, 2017,37(5):1483-1503.
52. Lambin P, Leijenaar R T H, Deist T M, et al. Radiomics: the bridge between medical imaging and personalized medicine [J]. Nature Reviews Clinical Oncology, 2017,14(12):749-762.
53. Eu E A F T, Live E A F T. EASL Clinical Practice Guidelines: Management of hepatocellular carcinoma. [J]. Journal of hepatology, 2018,69(1):182-236.
54. Management consensus guideline for hepatocellular carcinoma: 2016 updated by the Taiwan Liver Cancer Association and the Gastroenterological Society of Taiwan. [J]. Journal of the Formosan Medical Association = Taiwan yi zhi, 2018,117(5):381-403.
55. Lee Y J, Lee J M, Lee J S, et al. Hepatocellular carcinoma: diagnostic performance of multidetector CT and MR imaging-a systematic review and meta-analysis. [J]. Radiology, 2015,275(1):97-109.
56. Liu X, Jiang H, Chen J, et al. Gadoxetic acid disodium-enhanced magnetic resonance imaging outperformed multidetector computed tomography in diagnosing small hepatocellular carcinoma: A meta-analysis. [J]. Liver Transpl, 2017,23(12):1505-1518.
57. Choi S H, Lee S S, Kim S Y, et al. Intrahepatic Cholangiocarcinoma in Patients with Cirrhosis: Differentiation from Hepatocellular Carcinoma by Using Gadoxetic Acid-enhanced MR Imaging and Dynamic CT. [J]. Radiology, 2017,282(3):771-781.
58. Wei Y, Gao F, Zheng D, et al. Intrahepatic cholangiocarcinoma in the setting of HBV-related cirrhosis: Differentiation with hepatocellular carcinoma by using Intravoxel incoherent motion diffusion-weighted MR imaging. [J]. Oncotarget, 2018,9(8):7975-7983.
59. Lewis S, Peti S, Hectors S J, et al. Volumetric quantitative histogram analysis using diffusion-weighted magnetic resonance imaging to differentiate HCC from other primary liver cancers. [J]. Abdom Radiol (NY), 2019,44(3):912-922.
60. Wei M, Lü L, Lin P, et al. Multiple cellular origins and molecular evolution of intrahepatic cholangiocarcinoma. [J]. Cancer letters, 2016,379(2):253-261.
61. Peng J, Zheng J, Yang C, et al. Intravoxel incoherent motion diffusion-weighted imaging to differentiate hepatocellular carcinoma from intrahepatic cholangiocarcinoma. [J]. Scientific reports, 2020,10(1):7717.
62. Choi I Y, Lee S S, Sung Y S, et al. Intravoxel incoherent motion diffusion-weighted imaging for characterizing focal hepatic lesions: Correlation with lesion enhancement. [J]. J Magn Reson Imaging, 2017,45(6):1589-1598.
63. Shao S, Shan Q, Zheng N, et al. Role of Intravoxel Incoherent Motion in Discriminating Hepatitis B Virus-Related Intrahepatic Mass-Forming Cholangiocarcinoma from Hepatocellular Carcinoma Based on Liver

Imaging Reporting and Data System v2018. [J]. Cancer biotherapy & radiopharmaceuticals, 2019,34(8):511-518.
64. Çelebi F, Yaghouti K, Cindil E, et al. The Role of 18F-FDG PET/MRI in the Assessment of Primary Intrahepatic Neoplasms. [J]. Academic radiology, 2021,28(2):189-198.
65. Wang X, Wang S, Yin X, et al. MRI-based radiomics distinguish different pathological types of hepatocellular carcinoma. [J]. Computers in biology and medicine, 2022,141:105058.
66. Han X, Sun M, Wang M, et al. The enhanced T(2) star weighted angiography (ESWAN) value for differentiating borderline from malignant epithelial ovarian tumors. [J]. European journal of radiology, 2019,118:187-193.
67. Greiner M, Pfeiffer D, Smith R D. Principles and practical application of the receiver-operating characteristic analysis for diagnostic tests. [J]. Preventive veterinary medicine, 2000,45(1-2):23-41.
68. Fahmy D, Alksas A, Elnakib A, et al. The Role of Radiomics and AI Technologies in the Segmentation, Detection, and Management of Hepatocellular Carcinoma [J]. Cancers, 2022,14(24):6123.
69. Jiang C, Zhao L, Xin B, et al. 18F-FDG PET/CT radiomic analysis for classifying and predicting microvascular invasion in hepatocellular carcinoma and intrahepatic cholangiocarcinoma [J]. Quantitative Imaging in Medicine and Surgery, 2022,12(8):4135-4150.
70. Xu X, Mao Y, Tang Y, et al. Classification of Hepatocellular Carcinoma and Intrahepatic Cholangiocarcinoma Based on Radiomic Analysis [J]. Computational and Mathematical Methods in Medicine, 2022,2022:1-9.
71. Ren S, Li Q, Liu S, et al. Clinical Value of Machine Learning-Based Ultrasomics in Preoperative Differentiation Between Hepatocellular Carcinoma and Intrahepatic Cholangiocarcinoma: A Multicenter Study. [J]. Frontiers in oncology, 2021,11:749137.
72. Peng Y, Lin P, Wu L, et al. Ultrasound-Based Radiomics Analysis for Preoperatively Predicting Different Histopathological Subtypes of Primary Liver Cancer. [J]. Frontiers in oncology, 2020,10:1646.
73. Zhang J, Huang Z, Cao L, et al. Differentiation combined hepatocellular and cholangiocarcinoma from intrahepatic cholangiocarcinoma based on radiomics machine learning. [J]. Annals of translational medicine, 2020,8(4):119.
74. Gao R, Zhao S, Aishanjiang K, et al. Deep learning for differential diagnosis of malignant hepatic tumors based on multi-phase contrast-enhanced CT and clinical data. [J]. J Hematol Oncol, 2021,14(1):154.
75. Just N. Improving tumour heterogeneity MRI assessment with histograms. [J]. British journal of cancer, 2014,111(12):2205-2213.
76. Zhao Y, Chen W, Wu D, et al. Differentiation of mass-forming intrahepatic cholangiocarcinoma from poorly differentiated hepatocellular carcinoma: based on the multivariate analysis of contrast-enhanced computed tomography findings. [J]. Abdominal radiology (New York), 2016,41(5):978-989.